



ESA Climate Change Initiative – Fire_cci

O3.D5 Radar – Algorithm intercomparison document

Project Name	ECV Fire Disturbance: Fire_cci Phase 2
Contract N°	4000115006/15/I-NB
Issue Date	30/10/2018
Version	1.1
Author	Mihai A. Tanase, Miguel Ángel Belenguer Plomer, Ángel Fernández Carrillo, Ekhi Roteta, Aitor Bastarrika, James Wheeler, Kevin Tansey, Werner Wiedemann, Peter Navratil
Document Ref.	Fire_cci_O3.D5_AID-SFD-SA_v1.1
Document type	Public

To be cited as: M.A. Tanase, M.A. Belenguer Plomer, A. Fernández Carrillo, E. Roteta, A. Bastarrika, J. Wheeler, K. Tansey, W. Wiedemann, P. Navratil (2018) ESA CCI ECV Fire Disturbance: O3.D5 Radar – Algorithm intercomparison document, version 1.1. Available at: <http://www.esa-fire-cci.org/documents>



fire
cci

Fire_cci
Algorithm inter-comparison document

Ref.:	Fire_cci_O3.D5_AID-SFD-SA_v1.1		
Issue	1.1	Date	30/10/2018
Page	2		

Project Partners

Prime Contractor/ Scientific Lead & Project Management	UAH – University of Alcalá (Spain)
Earth Observation Team	UAH – University of Alcalá (Spain)
System Engineering	Cubenube (Spain)



Universidad
de Alcalá



Distribution

Affiliation	Name	Address	Copies
ESA	Stephen Plummer (ESA)	stephen.plummer@esa.int	electronic copy
Project Team	Emilio Chuvieco (UAH)	emilio.chuvieco@uah.es	electronic copy
	M. Lucrecia Pettinari (UAH)	mlucrecia.pettinari@uah.es	
	Joshua Lizundia (UAH)	joshua.lizundia@uah.es	
	Gonzalo Otón (UAH)	gonzalo.oton@uah.es	
	Mihai Tanase (UAH)	mihai.tanase@uah.es	
	Miguel Ángel Belenguer (UAH)	miguel.belenguer@uah.es	
	Aitor Bastarrika (EHU)	aitor.bastarrika@ehu.es	
	Ekhi Roteta (EHU)	ekhi.roteta@gmail.com	
	Kevin Tansey (UL)	kjt7@leicester.ac.uk	
	Marc Padilla Parellada (UL)	mp489@leicester.ac.uk	
	James Wheeler (UL)	jemw3@leicester.ac.uk	
	Philip Lewis (UCL)	ucfalew@ucl.ac.uk	
	José Gómez Dans (UCL)	j.gomez-dans@ucl.ac.uk	
	James Brennan (UCL)	james.brennan.11@ucl.ac.uk	
	Jose Miguel Pereira (ISA)	jmocpereira@gmail.com	
	Duarte Oom (ISA)	duarte.oom@gmail.com	
	Manuel Campagnolo (ISA)	mlc@isa.ulisboa.pt	
	Thomas Storm (BC)	thomas.storm@brockmann-consult.de	
	Johannes Kaiser (MPIC)	j.kaiser@mpic.de	
	Angelika Heil (MPIC)	a.heil@mpic.de	
Florent Mouillot (IRD)	florent.mouillot@cefe.cnrs.fr		
M. Vanesa Moreno (IRD)	mariavanesa.morenodominguez@cefe...		
Philippe Ciaï (LSCE)	philippe.ciaï@lsce.ipsl.fr		
Chao Yue (LSCE)	chaoyuejoy@gmail.com		
Pierre Laurent (LSCE)	pierre.laurent@lsce.ipsl.fr		
Guido van der Werf (VUA)	guido.vander.werf@vu.nl		
Ioannis Bistinas (VUA)	i.bistinas@vu.nl		



fire
cci

Fire_cci
Algorithm inter-comparison document

Ref.: Fire_cci_O3.D5_AID-SFD-SA_v1.1

Issue 1.1 Date 30/10/2018

Page 3

Summary

This document describes the performance of the burned area (BA) detection algorithm developed within the Option 3 over test sites in Indonesia and Africa. The results of the BA detection algorithms developed by RSS (Sentinel-1), UL (Sentinel-1), and EHU (Sentinel-2) were also tested using the same reference datasets to appraise the strengths and deficiencies of each of the algorithms developed within the small fire database (SFD) framework.

	Affiliation/Function	Name	Date
Prepared	UAH	Mihai A. Tanase, Miguel Ángel Belenguier Plomer, Ángel Fernández Carrillo	30/10/2018
	EHU	Ekhi Roteta, Aitor Bastarrika	
	UL	James Wheeler, Kevin Tansey	
	RSS	Werner Wiedemann, Peter Navratil	
Reviewed	UAH - Science Leader	Emilio Chuvieco	30/10/2018
	UAH – Project Manager	Lucrecia Pettinari	
Authorized	UAH - Science Leader	Emilio Chuvieco	30/10/2018
Accepted	ESA - Technical Officer	Stephen Plummer	30/10/2018

This document is not signed. It is provided as an electronic copy.

Document Status Sheet

Issue	Date	Details
1.0	23/05/2018	First Issue of the document
1.1	30/10/2018	Addressing comments of ESA-CCI-EOPS-FIRE-MM-18-0160

Document Change Record

Issue	Date	Request	Location	Details
1.1	30/10/2018	UAH	Section 2.2	New reference document added Section updated
		ESA	Section 5	

Table of Contents


1	Executive Summary	5
2	Introduction.....	6
2.1	Purpose of the document.....	6
2.2	Reference Documents	6
2.3	Background.....	6
3	Reference areas	7
3.1	UAH.....	9
3.2	EHU	9
3.3	RSS	10
4	BA algorithms inter-comparison	10
4.1	Africa	11
4.2	Indonesia.....	14
4.2.1	Perimeter-based inter-comparison.....	14
4.2.2	Grid-based inter-comparison	14
5	Conclusions.....	15
6	References	16
Annex 1: Acronyms and abbreviations		18
Annex 2a: BA detected by tiles, UAH algorithm. OE and CE errors are shown.		19
Annex 2b: BA detected by tiles, EHU algorithm. OE and CE errors are shown.		22
Annex 2c: BA detected by tiles, UL algorithm. OE and CE errors are shown.....		24
Annex 2d: BA detected by tiles, RSS algorithm. OE and CE errors are shown.....		26

List of Tables

Table 1:	MGRS tiles used for inter-comparison.....	9
Table 2:	Sampled error matrix on a sampling unit*.....	10
Table 3:	Agreement between reference and detected BA by algorithm and tile.....	11
Table 4:	Confusion matrices for all tiles by algorithm. Numbers represent pixel counts. Each tile has 7.5625 million pixels at 40 m spatial resolution.	13
Table 5:	Agreement between reference and detected BA by land cover type in Africa. ..	13
Table 6:	Agreement between reference and detected BA from fire perimeter validation.	14
Table 7:	Agreement between reference and detected BA from point-based validation. ...	14
Table 8:	Agreement between reference and detected BA by land cover type.....	15

List of Figures

Figure 1:	MGRS tiles used for inter-comparison in Arica (left panel) and Indonesia (right panel). The source of reference BA data is also shown.....	8
Figure 2:	Reference sample points used for the grid-based inter-comparison approach in Indonesia.....	8

	Fire_cci		Ref.: Fire_cci_O3.D5_AID-SFD-SA_v1.1
	Algorithm inter-comparison document		Issue 1.1 Date 30/10/2018
			Page 5

1 Executive Summary

Option 3 uses the systematically distributed Sentinel-1 Level-1 Ground Range Detected (GRD) data to detect burned areas within an automatic, locally adaptive detection algorithm. The algorithm is locally trained, by broad land cover classes, and uses a multi-temporal approach for the detection of anomalous changes with respect to a reference state. The training samples are selected using ancillary information (hotspots) from MODIS and VIIRS instruments. Detailed information on the Sentinel-1 system and the Burned Area (BA) algorithm developed within Option 3 are available in [RD-1].

This deliverable provides a comparative analysis between the Option 3 BA algorithm (henceforth UAH algorithm) and the algorithms developed for BA detection from high resolution Sentinel-1 and -2 datasets for the SFD as well as the algorithm developed for BA detection in Indonesia within the Special Case Study on Fires in Indonesia and El Niño. The algorithms were developed over


- 1) Africa from Sentinel-2 optical data (henceforth EHU algorithm)
- 2) Africa from Sentinel-1 interferometric coherence (henceforth UL algorithm)
- 3) Indonesia from Sentinel-1 backscatter coefficient (henceforth RSS algorithm)

Each algorithm was assessed in up to 12 test tiles in Africa. The tiles cover areas of Tropical Forests and Tropical and Subtropical Grasslands, Savannah and Shrublands biomes. Three of these tiles were part of the inter-comparison carried out by RSS as described in [RD-3]. In Indonesia, the algorithms developed by RSS and UAH were compared over four tiles that overlap the Tropical and Subtropical Moist Broadleaf Forest biome.

The performance of the algorithms was tested by evaluating the agreement with reference burned perimeters derived from Landsat 8 imagery (at UAH) and Sentinel-2 imagery (at EHU). The reference fire perimeters were generated through semi-automatic procedures. Manually delineated training polygons were used, within machine learning classification (UAH) or for establishing thresholds on spectral indices (EHU), to discriminate between burned/unburned areas. After the semi-automatic mapping, quality control was performed through visual inspection. Fire perimeters were reviewed and perimeters with errors were manually rectified. This procedure was iterated until no errors were identified. At each partner, one person was responsible for the generation of the reference BA perimeters. Multi-operator cross-accuracy tests were not carried on.

Accuracy estimates were based on the cross-tabulation approach. Overall, commission (CE) and omission errors (OE) were computed as well as the Dice coefficient and the relative bias for burned pixels. The comparison between Landsat/S-2 reference perimeters and S-1 results are a first estimation of S-1 performance, as marginal errors may still remain in reference perimeters, on one hand, and temporal mismatches between detected BA and the reference perimeters may artificially increase error estimates, on the other.

In Africa, the average omission and commission errors were 33% and 29% for the EHU algorithm (over 11 tiles), 60% and 37% for the UAH algorithm (over 12 tiles), and 99% and 46% for the RSS algorithm (over 3 tiles). For the UL coherence-based algorithm, the OE and CE reached 72% and 57% respectively. When the reference datasets were derived from independent sensors (i.e., Landsat 8) the omission and commission errors for the EHU algorithm were 40% and 50%, values similar with those observed for the UAH algorithm over largely the same tiles. In Indonesia, the UAH and RSS algorithms

	Fire_cci		Ref.: Fire_cci_O3.D5_AID-SFD-SA_v1.1
	Algorithm inter-comparison document		Issue 1.1 Date 30/10/2018
			Page 6

showed similar values for OE (18 vs 17%) while CE were slightly larger for the UAH algorithm (43 vs 32%) over the four tiles analysed.

2 Introduction

2.1 Purpose of the document

The objective of this document is to describe the inter-comparison results between the SFD algorithms using a common reference burned area dataset. The document provides a quantitative assessment of the algorithms accuracies using independent datasets. This document complements [RD-1] to [RD-5].


2.2 Reference Documents

[RD-1]	M. A. Tanase, M. A. Belenguer-Plomer (2017) ESA CCI ECV Fire Disturbance: O3.D1 Algorithm Theoretical Basis Document (ATBD) – Small Fires Dataset (SFD) for the large demonstrator area (LDA) in South America, v1.0.
[RD-2]	M. A. Tanase, M. A. Belenguer-Plomer (2018) ESA CCI ECV Fire Disturbance: O3.D3 Intermediate validation results: SAR pre-processing and burned area detection, v1.0.
[RD-3]	S. Lohberger, W. Wiedemann, F. Siegert (2017) ESA CCI ECV Fire Disturbance: O.RSS.D5 Algorithm Intercomparison Document, v1.1.
[RD-4]	A. Bastarrika, E. Roteta, K. Tansey, M. Padilla Parellada, J. Wheeler (2017) ESA CCI ECV Fire Disturbance: D2.1.2 Algorithm Theoretical Basis Document (ATBD) – Small Fires Dataset (SFD), v0.1.
[RD-5]	M. Padilla, J. Wheeler, K. Tansey (2017) ESA CCI ECV Fire Disturbance: D4.1.1 Product Validation Report (PVR), v1.3.
[RD-6]	M. A. Tanase, A. Fernández Carrillo (2018) ESA CCI ECV Fire Disturbance: O3.D2. Burned area database for candidate validation tiles, v1.1.
[RD-7]	M. Padilla, J. Wheeler and K. Tansey (2018) ESA CCI – Fire_cci D4.1.1 Product Validation Report (PVR)

2.3 Background

Global BA products are based on coarse resolution sensors (from 300 to 1000m). The likelihood of detecting small burns (i.e. < 50ha) is low in coarse resolution products with frequent omission errors being observed (Giglio et al. 2009; Padilla et al. 2015), particularly coming from small fires (Randerson et al. 2012). To improve the characterization of small fires, one of the objectives of the Fire_cci Phase 2 project is generating a small fires database using medium resolution sensors (10 to 100m). Considering the massive processing effort when generating products at global level, the SFD was focused on the African continent, the most burned worldwide (Chuvienco et al. 2016; Giglio et al. 2013), with additional areas being *a posteriori* selected over tropical South-east Asia and South America.

The BA algorithm developed in Option 3 uses temporal time-series of Sentinel-1 backscatter coefficient to identify changes and associate them with biomass burning. The algorithm considers multi-temporal changes of incoherent SAR-based metrics (e.g. backscatter intensities) together with ancillary information on land cover and active fires (hotspots). The Reed-Xiaoli detector (Reed and Yu 1993) is used to distinguish areas

	Fire_cci		Ref.: Fire_cci_O3.D5_AID-SFD-SA_v1.1
	Algorithm inter-comparison document		Issue 1.1 Date 30/10/2018
			Page 7

affected by anomalous changes (AC) with respect to a reference state provided by Sentinel-1 acquired before the period of interest. When hotspots coincide in space and time with ACs these areas are labelled as burned. The remaining ACs are labelled as burned/unburned using Random Forests (RF). The RFs are trained locally (MGRS tiles) by main land cover types (e.g. crops, forests). RF training samples are obtained using the ACs with overlapping hotspots after applying a series of filtering mechanisms to ensure high burned/unburned probabilities of the selected samples [RD-1]. The algorithm was developed and tested over seven tiles located in tropical South America. In addition, the algorithm performance was tested over 18 tiles located worldwide. The additional testing revealed minor deficiencies which helped improving the robustness of the algorithm.

The EHU detection algorithm is based on time-series of atmospherically corrected Sentinel-2 reflectance from three bands (NIR, SWIR1, and SWIR12) at the original spatial resolution of 20m. These bands are used to calculate two spectral indices the Mid-Infrared Burned Index (MIRBI) and the Normalized Burned Ratio 2 (NBR2). The algorithm compares two Sentinel 2 images using the multitemporal difference and the post values of the MIRBI, NBR2 spectral indices and the NIR. The algorithm applies a fixed threshold to obtain an *Initial Burned/Not Burned* area which is cross-checked against the existence of MODIS active fire hotspots. When hotspots exist, the Initial Burned/Not Burned is confirmed (IBC). IBC areas are used to select burned seeds which are subsequently used to derive a burned membership function, where the minimum and maximum values are extracted from unburned background and burned areas [RD-4].

The UL detection algorithm is based on Sentinel-1 interferometric coherence time-series and needs 4 consecutive acquisitions (12 days apart) of the study area to identify burns over the period of interest. For each period of interest, the algorithm generates three interferometric products corresponding to pre-, fire, and post-fire epochs. The post-fire epoch is used to cross-check that burns have indeed taken place. The algorithm uses pre-trained machine learning algorithms (Random Forests). The training is based on manually selected polygons for four classes (no data, burned, unburned and water). The pre-trained algorithms are biome specific [RD-4].

The RSS detection algorithm is based on Sentinel-1 datasets acquired at the beginning and the end of the fire season. The selection of such Sentinel-1 images is based on MODIS Active Fires as well as on precipitation data from the Tropical Rainfall Measuring Mission (TRMM). TRMM is used to select Sentinel-1 data not affected by rainfall, an important source of variability affecting the backscatter intensity. The BA detection is based on image segmentation and object-based image analysis and classification. As input for segmentation, the backscatter intensities acquired before and after the fire season, as well as their ratios, are used. The objects are then classified based on probabilities of belonging to the class “burned area”, produced from mean fuzzy logic threshold values for backscatter and temporal change metric layers, as well as neighbourhood features and hierarchical relationships. One should note that, as opposed to the remaining algorithms, the RSS approach does not provide for an approximate date of burning as only two Sentinel-1 dates were used, one before the fire season and one after.

3 Reference areas

Since inference processes (models) are affected by errors there is an element of uncertainty regarding the results produced using remote sensing data. Therefore, the

quality of remote sensing data and the derived products needs to be characterized quantitatively to facilitate critical information on product reliability to end users. Accuracy of the results is usually characterized through cross-tabulation against reference datasets by accounting for the spatio-temporal coincidences and disagreements. The approach is widely used in BA mapping projects (Boschetti et al. 2004; Boschetti et al. 2009; Boschetti et al. 2016; Chuvieco et al. 2008; Giglio et al. 2009; Padilla et al. 2017; Padilla et al. 2014; Padilla et al. 2015; Roy and Boschetti 2009). One should bear in mind that cross-tabulation based on ancillary reference datasets derived from remote sensing data acquired by other sensors, largely indicates the agreement between BA products as the accuracy of the reference dataset is not known. In addition, mismatches between sensors passes may results in disagreements of the detected burned area due to the different acquisition dates.

Reference burned perimeters were available from two different sources, UAH and EHU (Figure 1). In addition, for the Indonesian test site, a validation grid based on randomly sampled points was also available from RSS (Figure 2). The MGRS tile selected for the inter-comparison exercise are presented in Table 1.

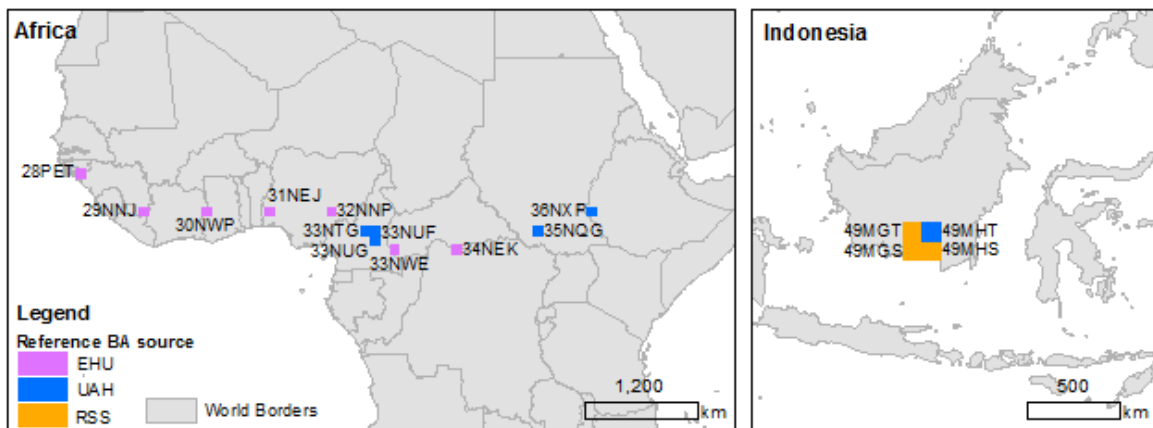


Figure 1: MGRS tiles used for inter-comparison in Arica (left panel) and Indonesia (right panel). The source of reference BA data is also shown.

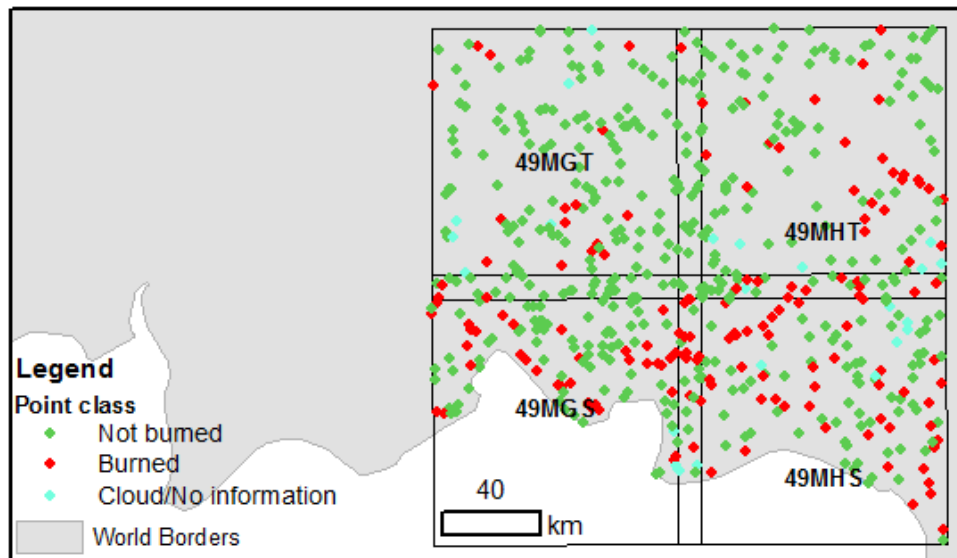


Figure 2: Reference sample points used for the grid-based inter-comparison approach in Indonesia



Table 1: MGRS tiles used for inter-comparison

MGRS tile	Reference data source	Cover type	Available BA detections:	MGRS tile	Reference data source	Cover type	Available BA detections:
28PET ^S	EHU	S, F	EHU, UL, UAH	33NWE ^S	EHU	F, S	EHU, UL, UAH
29NNJ ^S	EHU	F	EHU, UL, UAH	34NEK ^S	EHU	F	EHU, UL, UAH
30NWP ^S	EHU	F, S	EHU, UL, UAH	35NQG ^L	UAH	S, F	EHU, UL, UAH
31NEJ ^S	EHU	S, F	EHU, UL, UAH	36NXP ^L	UAH	S	EHU, UL, UAH
32NNP ^S	EHU	S	EHU, UL, UAH	49MHT ^{LS}	UAH / RSS ¹	F	RSS, UAH
33NTG ^L	UAH	S, F	EHU, UL, RSS, UAH	49MGS	RSS ¹	F, M	RSS, UAH
33NUF ^L	UAH	F, S	EHU, UL, RSS, UAH	49MGT	RSS ¹	F	RSS, UAH
33NUG ^L	UAH	S	EHU, UL, RSS, UAH	49MHS	RSS ¹	F, M	RSS, UAH

¹ Point reference data. See section 3.3 for details. F- Tropical and subtropical forest, S – Tropical and subtropical savanna, grasslands, shrublands, M- Mangroves. The sensor used to generate the reference fire perimeters was labelled by the MGRS tile as: S for Sentinel-2 and L for Landsat-8.

3.1 UAH

Reference burn perimeters over six tiles, five in Africa and one in Indonesia (Table 1) were generated using multi-temporal Landsat 8 images as detailed in [RD-6]. Largely, the process consists in two steps. First, surface reflectance of each individual image pair is reformatted for efficiency. The output is a raster file containing six bands (i.e., the SWIR, NIR and RED bands of each image forming the pair). Second, the interpreter digitizes training polygons for burned and unburned areas, and optionally for clouds. The polygons are used to train a Random Forest Classifier (Breiman 2001; Pedregosa et al. 2011), taking as input variables the pre- and post-reflectance and the multitemporal dNBR index. The classification procedure consists in repetitive iterations of visual inspection, delineation of training polygons, and classification until no further errors can be perceived. When needed, the classification was improved by digitizing missed areas. Within post-processing, the detected perimeters were filtered with polygons below 0.1 ha being removed. Shape indices were used to reduce misclassification errors over cropping areas. A filter based on shape indices and size was applied to all polygons below 2 ha.

Parts of the scene that cannot be observed or interpreted, due to either clouds or shadows were classified as no-data. As such, only areas with reliable information are included in the validation process. Sentinel-2 data are used (when available) for gap filling the temporal series of reference perimeters during the fire season when Landsat 8 images are separated by more than two cycles (32 days).

3.2 EHU

Reference burn perimeters for 52 tiles were provided by EHU. Seven were selected for the inter-comparison exercise in Africa (Figure 1 and Table 1). The tiles were selected on an east-west transect to i) coincide with the latitude of the MGRS tiles for which reference data from UAH were available and ii) provide for a diverse land cover.

In each validation area, two Sentinel-2 cloud-free images with a temporal difference as short as possible were selected, in a period where fires were visually observed. L1C products from these dates were downloaded and processed with sen2cor to obtain L2A products, which contain Bottom-of-Atmosphere reflectance and a scene classification.

From these pre-fire and post-fire images, reference perimeters were generated using the Burned Area Mapping Software (BAMS) (Bastarrika et al. 2014). First training polygons were defined. BAMS was subsequently run and results were visually analysed. The training polygons were modified until acceptable results were obtained. Polygons not corresponding to burned areas were removed manually, with most being caused by cloud shadows and crop harvest.

3.3 RSS

The RSS validation grid for the Indonesian test site was derived based on the visual assessment of Landsat-8 and Sentinel-2 images. For each MGRS tile (i.e., 49MHT, 49MGS, 49MHS, and 49MGT), 150 random points were evaluated (Figure 2). Each point was assigned to ‘burned’ or ‘unburned’ classes. The date of BA detection was assigned as the date of burn. Points falling in areas covered by clouds or with no information available were assigned to the class ‘cloud/no information’.

4 BA algorithms inter-comparison

For each tile, the agreement between the reference and the detected burned areas was computed through cross-tabulation (Latifovic and Olthof 2004). The detected BA products were matched to the reference BA perimeter dates as closely as possible. Notice that a perfect matching of dates was possible only between the EHU BA product and EHU reference product (fire perimeter) as the same sensor was used when generating both products. For the remaining algorithms detection and validation periods differed. The result of the cross tabulation can be represented by the error matrix (Table 2) which express the amount of agreement between a product and a reference classification.

Table 2: Sampled error matrix on a sampling unit*.

Product	Reference		Total
	Burned	Unburned	
Burned	e_{11}	e_{12}	e_{1+}
Unburned	e_{21}	e_{22}	e_{2+}
Total	e_{+1}	e_{+2}	

* e_{ij} express the agreements (diagonal cells) or disagreements (off diagonal cells) in terms of area (m^2) between the BA product (map) class and the reference class

From the confusion matrix, commission (CE, Eq.1) and omission errors (OE, Eq. 2) and the Dice coefficient (DC, Eq.3) were computed. DC summarizes both commission and omission errors showing the global accuracy for the target category. In addition, the bias was computed in relative terms to the reference BA (Eq. 4).

$$Ce = \frac{e_{12}}{e_{1+}} \quad (1); \quad Oe = \frac{e_{21}}{e_{+1}} \quad (2); \quad DC = \frac{2e_{11}}{2e_{11} + e_{12} + e_{21}} \quad (3); \quad relB = \frac{e_{12} - e_{21}}{e_{+1}} \quad (4)$$

The validation metrics were computed as an aggregate over each tile as well as by main land cover classes (i.e., forest, savannas/grasslands/shrubland, and mangroves). The CCI Land Cover product v2.0.7 for the year 2015 (Santoro et al. 2017) was used to segment the area by main land cover types. In addition, aggregate metrics for all tiles detected by each BA algorithm (by continent) were computed. Note that cloud affected area, no data areas, and Sentinel 1/2 pre-processing errors were masked out and were not used when computing the accuracy metrics.



4.1 Africa

Between three and 11 tiles were available for comparison in Africa depending on the algorithm. Although the reference validation periods were common, the detection periods varied depending on the algorithm input data (e.g., Sentinel-1, Sentinel-2) thus precluding a like for like comparison. However, general trends may be distinguished particularly for the UAH, UL, and EHU algorithms, which have been tested over more areas (Table 3). At a first glance, the EHU Sentinel-2 algorithm seems superior over the Sentinel-1 algorithms although for particular tiles (35NQG, 36NXP) this was not the case. Over all tiles, the EHU algorithm showed OE and CE around 30% while for the UAH algorithm the OE and CE were around 60% and 40% respectively. The coherence-based UL algorithm showed slightly higher OE (72%) and CE (57%) errors when compared to the backscatter-based UAH algorithm. The RSS Sentinel-1 algorithm showed much higher OE with the average value over the three analysed tiles being 99%. The large omission errors may be the result of fine tuning the RSS algorithm over tropical forests and the predominance of grasslands in the three tiles analysed.

Much higher accuracies were obtained for the EHU algorithm over tiles where the validation data were generated from Sentinel-2 images (Table 3). Over tiles where the validation data was generated from Landsat-8 images the EHU algorithm showed OE and CE estimates in the same range as those observed for the UAH algorithm (40 to 50% on average). The low OE (10% on average) and CE errors (20% on average) observed for the EHU algorithm when using Sentinel-2 based validation perimeters was attributed to i) exact matching of validation and detection periods thus avoiding errors due to missing or extra days; ii) the same spatial resolution (20 m) at which validation and detection were carried out and thus lower errors along fire borders; iii) use of the same spectral information (Sentinel 2 bands); iv) similarities between the BAMS algorithm (used for validation perimeters) and the EHU algorithm.

By land cover type (Table 5), the EHU algorithm showed small average OE and CE over cropping areas (15%) and forests (13% to 29%) while for the UAH algorithm the errors were largely similar over most classes (34-50%). From Table 3 and Table 4 the average classification rates (classified vs. not classified) were computed for each algorithm. The not classified areas corresponded to areas of no data (e.g., lack of satellite images), clouds/shadows (for the Sentinel 2 algorithm) or pre-processing errors (e.g., difficulties in derive coherence estimates). The classification rates for UAH, EHU, UL and RSS algorithms were 75%, 68%, 66% and 78% respectively. Note that classification rates do not reach 100% of the analysed tiles as the reference perimeters contain no data due to clouds and shadows.

Table 3: Agreement between reference and detected BA by algorithm and tile.

MGRS tile	Validation period	Detection period	OA	OE	CE	DC	relB
UAH							
28PET ^S	11.01.2016-11.03.2016	08.01.2016-08.03.2016	0.91	0.69	0.17	0.45	-0.62
29NNJ ^S	02.01.2016-02.03.2016	29.12.2015-10.03.2016	0.94	0.24	0.31	0.73	0.10
30NWP ^S	27.12.2015-16.01.2016	21.12.2015-16.01.2016	0.96	0.45	0.24	0.64	-0.28
31NEJ ^S	18.12.2015-07.01.2016	18.12.2015-07.01.2016	0.92	0.87	0.62	0.19	-0.66
32NNP ^S	22.12.2015-10.02.2016	22.12.2015-10.02.2016	0.74	0.79	0.30	0.33	-0.69
33NTG ^L	28.11.2015-16.02.2016	21.11.2015-13.02.2016	0.90	0.46	0.22	0.64	-0.30
33NTGb ^L	15.01.2016-16.02.2016	08.01.2016-13.02.2016	0.96	0.55	0.48	0.48	-0.12



MGRS tile	Validation period	Detection period	OA	OE	CE	DC	relB
33NUF ^L	07.12.2015-23.12.2015	28.11.2015-22.12.2015	1.00	0.51	0.43	0.53	-0.13
33NUG ^L	21.11.2015-24.01.2016	16.11.2015-21.01.2016	0.96	0.52	0.44	0.52	-0.14
33NUGb ^L	22.10.2016-10.01.2017	17.10.2016-10.01.2017	0.94	0.44	0.32	0.62	-0.17
33NUGc ^L	22.10.2016-25.12.2016	16.11.2016-28.12.2016	0.97	0.53	0.34	0.55	-0.30
33NWE ^S	02.01.2016-22.01.2016	22.12.2015-22.01.2016	0.92	0.24	0.47	0.63	0.44
35NQG ^L	01.11.2016-19.12.2016	31.10.2016-19.12.2016	0.73	0.59	0.44	0.47	-0.27
36NXP ^L	9.09.2016-12.11.2016	27.09.2016-15.11.2016	0.99	0.13	0.91	0.16	8.83
36NXPb ^L	30.12.2016-15.01.2017	1.01.2017-26.01.2017	0.86	0.59	0.42	0.48	-0.29
All tiles	N/A	N/A	0.90	0.60	0.37	0.49	-0.36
RSS							
33NTG ^L	28.11.2015-16.02.2016	28.11.2015-20.02.2016	0.83	0.99	0.54	0.01	-0.99
33NUF ^L	07.12.2015-23.12.2015	10.12.2015-22.12.2015	1.00	0.96	0.39	0.07	-0.94
33NUG ^L	21.11.2015-24.01.2016	28.11.2016-27.01.2016	0.95	0.96	0.41	0.08	-0.93
All tiles	N/A	N/A	0.92	0.99	0.46	0.03	-0.97
EHU							
28PET ^S	11.01.2016-11.03.2016	11.01.2016-11.03.2016	0.96	0.38	0.02	0.76	-0.37
29NNJ ^S	02.01.2016-02.03.2016	02.01.2016-02.03.2016	0.95	0.09	0.33	0.78	0.35
30NWP ^S	27.12.2015-16.01.2016	27.12.2015-16.01.2016	0.99	0.16	0.03	0.90	-0.14
31NEJ ^S	18.12.2015-07.01.2016	18.12.2015-07.01.2016	0.98	0.16	0.09	0.87	-0.07
32NNP ^S	22.12.2015-10.02.2016	22.12.2015-10.02.2016	0.94	0.14	0.08	0.89	-0.06
33NTGb ^L	15.01.2016-16.02.2016	25.01.2016-14.02.2016	0.97	0.48	0.36	0.58	-0.19
33NUGc ^L _{HE}	22.10.2016-25.12.2016	21.10.2016-20.12.2016	0.96	0.98	0.37	0.04	-0.96
33NWE ^S	02.01.2016-22.01.2016	02.01.2016-22.01.2016	0.97	0.23	0.02	0.87	-0.21
34NEK ^S	27.12.2015-26.01.2016	27.12.2015-26.01.2016	0.98	0.22	0.03	0.87	-0.19
35NQG ^L	01.11.2016-19.12.2016	2.11.2016-22.12.2016	0.62	0.61	0.64	0.37	0.09
36NXPc ^L	13.01.2016-1.03.2016	11.01.2016-11.03.2016	0.78	0.79	0.55	0.14	4.30
36NXP ^L	9.09.2016-12.11.2016	7.09.2016-16.11.2016	0.99	0.56	0.92	0.28	-0.54
All tiles	N/A	N/A	0.92	0.33	0.29	0.69	-0.05
UL							
28PET ^S	11.01.2016-11.03.2016	2012.12.30-2016.03.23	0.89	0.91	0.45	0.16	-0.83
29NNJ ^S	02.01.2016-02.03.2016	2015.12.21-2016.03.14	0.91	0.93	0.23	0.14	-0.91
30NWP ^S	27.12.2015-16.01.2016	2015.12.15-2016.01.28	0.93	0.81	0.55	0.27	-0.58
31NEJ ^S	18.12.2015-07.01.2016	2015.12.06-2016.01.19	0.92	0.98	0.91	0.03	-0.81
32NNP ^S	22.12.2015-10.02.2016	2015.12.10-2016.02.22	0.62	0.60	0.63	0.38	0.08
33NTG ^L	28.11.2015-16.02.2016	2015.11.16-2016.02.28	0.84	0.75	0.45	0.34	-0.55
33NUF ^L	07.12.2015-23.12.2015	2015.11.25-2016.01.04	0.99	0.98	0.64	0.04	-0.95
33NUG ^L	21.11.2015-24.01.2016	2015.11.09-2016.02.05	0.95	0.97	0.43	0.07	-0.94
33NUGb ^L	22.10.2016-10.01.2017	2016.10.10-2017.01.22	0.91	0.99	0.37	0.03	-0.98
33NWE ^S	02.01.2016-22.01.2016	2015.12.21-2016.02.03	0.88	0.95	0.57	0.10	-0.88
35NQG ^L	01.11.2016-19.12.2016	2016.10.20-2016.12.31	0.66	0.19	0.49	0.63	0.59
36NXP ^L	9.09.2016-12.11.2016	2016.08.28-2016.11.24	1.00	0.94	0.71	0.11	-0.78
All tiles	N/A	N/A	0.87	0.72	0.57	0.34	-0.36

L- validation data from Landsat 8 images; S-validation data from Sentinel-2 images; HE- the particularly high errors seem to be caused by insufficient Sentinel-2 images; a, b, c letters in the MGRS tile name indicate different detection periods.



fire
cci

Fire_cci
Algorithm inter-comparison document

Ref.: Fire_cci_O3.D5_AID-SFD-SA_v1.1

Issue 1.1 Date 30/10/2018

Page 13

Table 4: Confusion matrices for all tiles by algorithm. Numbers represent pixel counts. Each tile has 7.5625 million pixels at 40 m spatial resolution.

UAH				EHU			
	Reference				Reference		
Detected	Burned	Unburned	Total	Detected	Burned	Unburned	Total
Burned	4133654	2427537	6561191	Burned	5269442	2194184	7463626
Unburned	6063518	72695392	78758910	Unburned	2573773	51872725	54446498
Total	10197172	75122929	85320101	Total	7843215	54066909	61910124

RSS				UL			
	Reference				Reference		
Detected	Burned	Unburned	Total	Detected	Burned	Unburned	Total
Burned	21550	17988	39538	Burned	1978967	2578989	4557956
Unburned	1436789	16256145	17692934	Unburned	5134371	50195430	55329801
Total	1458339	16274133	17732472	Total	7113338	52774419	59887757

Table 5: Agreement between reference and detected BA by land cover type in Africa.

Algorithm	Land cover	OA	OE	CE	DC	relB	Land cover (%)
UAH	Crops	0.92	0.62	0.35	0.48	-0.42	16
	Grasslands	0.97	0.71	0.49	0.37	-0.43	2
	Shrubs	0.84	0.62	0.40	0.47	-0.37	23
	Forests	0.93	0.54	0.35	0.54	-0.30	58
	Others	0.94	0.49	0.41	0.55	-0.13	1
	Non-burnable	0.97	0.99	0.30	0.02	-0.99	1
EHU	Crops	0.97	0.15	0.14	0.86	-0.01	23
	Grasslands	0.96	0.24	0.51	0.60	0.57	2
	Shrubs	0.83	0.44	0.45	0.55	0.02	18
	Forests	0.96	0.29	0.13	0.79	-0.18	55
	Others	0.98	0.29	0.04	0.82	-0.27	1
	Non-burnable	0.98	0.30	0.50	0.58	0.41	1
UL	Crops	0.93	1.00	0.46	0.01	12.06	21
	Grasslands	0.96	1.00	N/A	N/A	24.22	2
	Shrubs	0.96	0.97	0.13	0.06	3.47	19
	Forests	0.95	0.98	0.10	0.05	1.61	56
	Others	1.00	N/A	N/A	N/A	-0.45	1
	Non-burnable	0.89	1.00	N/A	N/A	1.26	1
RSS	Crops	0.98	0.90	0.22	0.17	-0.87	2
	Grasslands	0.99	1.00	N/A	0.00	-1.00	1
	Shrubs	0.90	0.99	0.53	0.03	-0.97	15
	Forests	0.92	0.99	0.44	0.03	-0.97	82
	Others	0.96	0.87	0.05	0.23	-0.86	0
	Non-burnable	0.96	0.98	0.63	0.04	-0.94	0

4.2 Indonesia

4.2.1 Perimeter-based inter-comparison

As expected, the RSS algorithm performed significantly better over the tropical forests of Indonesia with OE errors being generally low (22%) over the analysed tile (Table 6). The high CE observed for the RSS algorithm were likely related to the larger span of the detection period when compared to the validation dataset. The UAH algorithm performed reasonably well over the test Indonesian tile with the OE being similar with those recorded for the RSS algorithm (26 vs 22%). Again, the higher CE may be partially caused by the larger detection interval.

Table 6: Agreement between reference and detected BA from fire perimeter validation.

Algorithm	MGRS tile	Validation period	Detection period	OA	OE	CE	DC	relB
UAH	49MHT	02.07.2015-04.09.2015	26.06.2015-13.09.2015	0.94	0.26	0.39	0.67	0.21
RSS	49MHT ¹	02.07.2015-04.09.2015	20.07.2015-24.10.2015	0.73	0.22	0.79	0.33	2.7

¹notice the mismatch between detection and validation periods

4.2.2 Grid-based inter-comparison

The grid-based validation (Table 7) showed that RSS and UAH algorithms perform similarly over the tropical forests of Kalimantan with CE being almost identical (17% vs 18%). However, larger overall OE were observed for the UAH algorithm (43 vs 32%). At tile level, OE and CE varied between 15 and 55% for the UAH algorithm and 10 to 49% for the RSS algorithm. By land cover type (Table 8), the lowest errors were observed over forested areas for both algorithms with BA in flooded forests being particularly well detected by the UAH algorithm.

Table 7: Agreement between reference and detected BA from point-based validation.

Algorithm	MGRS tile	Validation period	Detection period	OA	OE	CE	DC	relB
UAH	49MGS	13.10.2015-26.12.2015	26.06.2015-11.12.2015	0.83	0.35	0.15	0.73	-0.23
	49MGT	13.10.2015-26.12.2015	26.06.2015-11.12.2015	0.96	0.20	0.20	0.80	0.00
	49MHS	13.09.2015-26.12.2015	26.06.2015-18.12.2015	0.74	0.55	0.22	0.57	-0.42
	49MHT	04.09.2015-09.12.2015	26.06.2015-18.12.2015	0.88	0.48	0.17	0.64	-0.38
	All	N/A	N/A	0.85	0.43	0.18	0.67	-0.30
RSS	49MGS	13.10.2015-26.12.2015	20.07.2015-31.10.2015	0.92	0.10	0.13	0.89	0.04
	49MGT	13.10.2015-26.12.2015	20.07.2015-31.10.2015	0.96	0.40	0.00	0.75	-0.40
	49MHS	13.09.2015-26.12.2015	20.07.2015-31.10.2015	0.73	0.49	0.28	0.60	-0.29
	49MHT	04.09.2015-09.12.2015	20.07.2015-31.10.2015	0.91	0.34	0.14	0.75	-0.24
	All	N/A	N/A	0.88	0.32	0.17	0.75	-0.18

Table 8: Agreement between reference and detected BA by land cover type.

Algorithm	Land cover	OA	OE	CE	DC	relB
UAH	Crops	0.79	0.43	0.11	0.70	-0.36
	Forest	0.90	0.40	0.24	0.68	-0.21
	Flooded forest	0.95	0.25	0.25	0.75	0.00
RSS	Crops	0.79	0.36	0.19	0.72	-0.21
	Forest	0.95	0.21	0.11	0.84	-0.12
	Flooded forest	0.95	0.25	0.25	0.75	0.00

5 Conclusions

The four algorithms compared here were developed using diverse input datasets (optic, radar backscatter, and interferometric coherence) and change detection strategies. When compared to reference fire perimeters derived from independent sensors (i.e., Landsat-8) the EHU and UAH algorithms provided similar results over the African tiles analysed. Over tiles where Sentinel-2 images were used to derive the validation perimeters, the BA detection accuracy improved noticeably for EHU algorithm (based on Sentinel-2 images) when compared to tiles for which the reference perimeters were derived from Landsat images. The Sentinel-1 coherence-based algorithm showed larger errors when compared to the backscatter-based UAH algorithm over all areas. The RSS algorithm behaved as expected in the tropical forests of Indonesia but was less accurate over the African savannas and grasslands, which may be attributed to the use of only two datasets at the beginning and the end of the fire season and the more dynamic recovery processes outside forest vegetation class.

One should notice, however, that accuracy metrics for the FireCCISFD11 product (based on the EHU algorithm) in Sub-Saharan Africa were high (DC=0.77, OE=0.27, CE=0.19) which suggest that tiles selected for algorithms inter-comparison in this report may not properly represent burn conditions over the entire Africa. Such an assumption is further supported by the much higher accuracy observed for the FIRECCIS1A10 (DC=0.48, OE=0.53, CE=0.57) product (based on the UL coherence algorithm) when assessed over a significantly larger area in Sub-Saharan Africa [RD-7].

Among the four algorithms it was clear that optical based algorithms may provide for a significant increase in accuracy over SAR based algorithms, particularly over regions where persistent cloud cover is not an issue. The radar-based algorithms provided accuracy metrics similar or better when compared to the most accurate global products currently available, the MCD64 and FIRECCI51. Furthermore, it is important to highlight that BA detection from SAR time series is in its infancy when compared to the decades long research based on optical sensors. Therefore, more mature SAR BA detection algorithms may provide accuracy metrics similar to those obtained from high resolution optical data (e.g. Sentinel-2) by taking advantage of combined backscatter-coherence information. Nevertheless, the added complexity of SAR data interpretation and the huge amount of data generated by interferometric SAR processing may only be justified over areas of persistent cloud cover where optical based algorithms may struggle due to cloud free data availability.



6 References

- Bastarrika, A., Alvarado, M., Artano, K., Martinez, M.P., Mesanza, A., Torre, L., Ramo, R., & Chuvieco, E. (2014). BAMS: A Tool for Supervised Burned Area Mapping Using Landsat Data. *Remote Sensing*, 6, 12360-12380
- Boschetti, L., Flasse, S.p.P., & Brivio, P.A. (2004). Analysis of the conflict between omission and commission in low spatial resolution dichotomic thematic products: The Pareto Boundary. *Remote Sensing of Environment*, 91, 280-292
- Boschetti, L., Roy, D., & Justice, C.O. (Eds.) (2009). *International Global Burned Area Satellite Product Validation Protocol. Part I – production and standardization of validation reference data*. USA: Committee on Earth Observation Satellites
- Boschetti, L., Stehman, S.V., & Roy, D.P. (2016). A stratified random sampling design in space and time for regional to global scale burned area product validation. *Remote Sensing of Environment*, 186, 465-478
- Breiman, L. (2001). Random Forests. *Machine Learning*, 45, 5-32
- Chuvieco, E., Opazo, S., Sione, W., Del Valle, H., Anaya, J., Di Bella, C., Cruz, I., Manzo, L., López, G., Mari, N., González-Alonso, F., Morelli, F., Setzer, A., Csiszar, I., Kanpandegi, J.A., Bastarrika, A., & Libonati, R. (2008). Global Burned Land Estimation in Latin America using MODIS Composite Data. *Ecological Applications*, 18, 64-79
- Chuvieco, E., Yue, C., Heil, A., Mouillot, F., Alonso-Canas, I., Padilla, M., Pereira, J.M., Oom, D., & Tansey, K. (2016). A new global burned area product for climate assessment of fire impacts. *Global Ecology and Biogeography*, 25, 619-629
- Giglio, L., Loboda, T., Roy, D.P., Quayle, B., & Justice, C.O. (2009). An active-fire based burned area mapping algorithm for the MODIS sensor. *Remote Sensing of Environment*, 113, 408-420
- Giglio, L., Randerson, J.T., & Werf, G.R. (2013). Analysis of daily, monthly, and annual burned area using the fourth generation global fire emissions database (GFED). *Journal of Geophysical Research: Biogeosciences*, 118, 317-328
- Latifovic, R., & Olthof, I. (2004). Accuracy assessment using sub-pixel fractional error matrices of global land cover products derived from satellite data. *Remote Sensing of Environment*, 90, 153-165
- Padilla, M., Olofsson, P., Stephen V., S., Tansey, K., & Chuvieco, E. (2017). Stratification and sample allocation for reference burned area data. *Remote Sensing of Environment*, in press
- Padilla, M., Stehman, S.V., & Chuvieco, E. (2014). Validation of the 2008 MODIS-MCD45 global burned area product using stratified random sampling. *Remote Sensing of Environment*, 144, 187-196
- Padilla, M., Stehman, S.V., Hantson, S., Oliva, P., Alonso-Canas, I., Bradley, A., Tansey, K., Mota, B., Pereira, J.M., & Chuvieco, E. (2015). Comparing the Accuracies of Remote Sensing Global Burned Area Products using Stratified Random Sampling and Estimation. *Remote Sensing of Environment*, 160, 114-121
- Pedregosa, F.V.G., Gramfort, A., Michel, V., Thirion, B., Grisel, O., Blondel, M., Prettenhofer, P., Weiss, R., Dubourg, V., Vanderplas, J., Passos, A., Cournapeau, D.,



fire
cci

Fire_cci
Algorithm inter-comparison document

Ref.: Fire_cci_O3.D5_AID-SFD-SA_v1.1

Issue 1.1 Date 30/10/2018

Page 17

Brucher, M., Perrot, M., & Duchesnay, E. (2011). Scikit-learn: Machine Learning in Python. *Journal of Machine Learning*, 12, 2825-2830

Randerson, J., Chen, Y., Werf, G., Rogers, B., & Morton, D.C. (2012). Global burned area and biomass burning emissions from small fires. *Journal of Geophysical Research: Biogeosciences*, 117-G04012, 1-23

Reed, I.S., & Yu, X. (1993). Adaptive multiple-band CFAR detection of an optical pattern with unknown spectral distribution. *IEEE Transactions on Acoustics, Speech, and Signal Processing*, 38, 1760-1770

Roy, D.P., & Boschetti, L. (2009). Southern Africa validation of the MODIS, L3JRC, and GlobCarbon burned-area products. *IEEE Transactions on Geoscience and Remote Sensing*, 47, 1032-1044

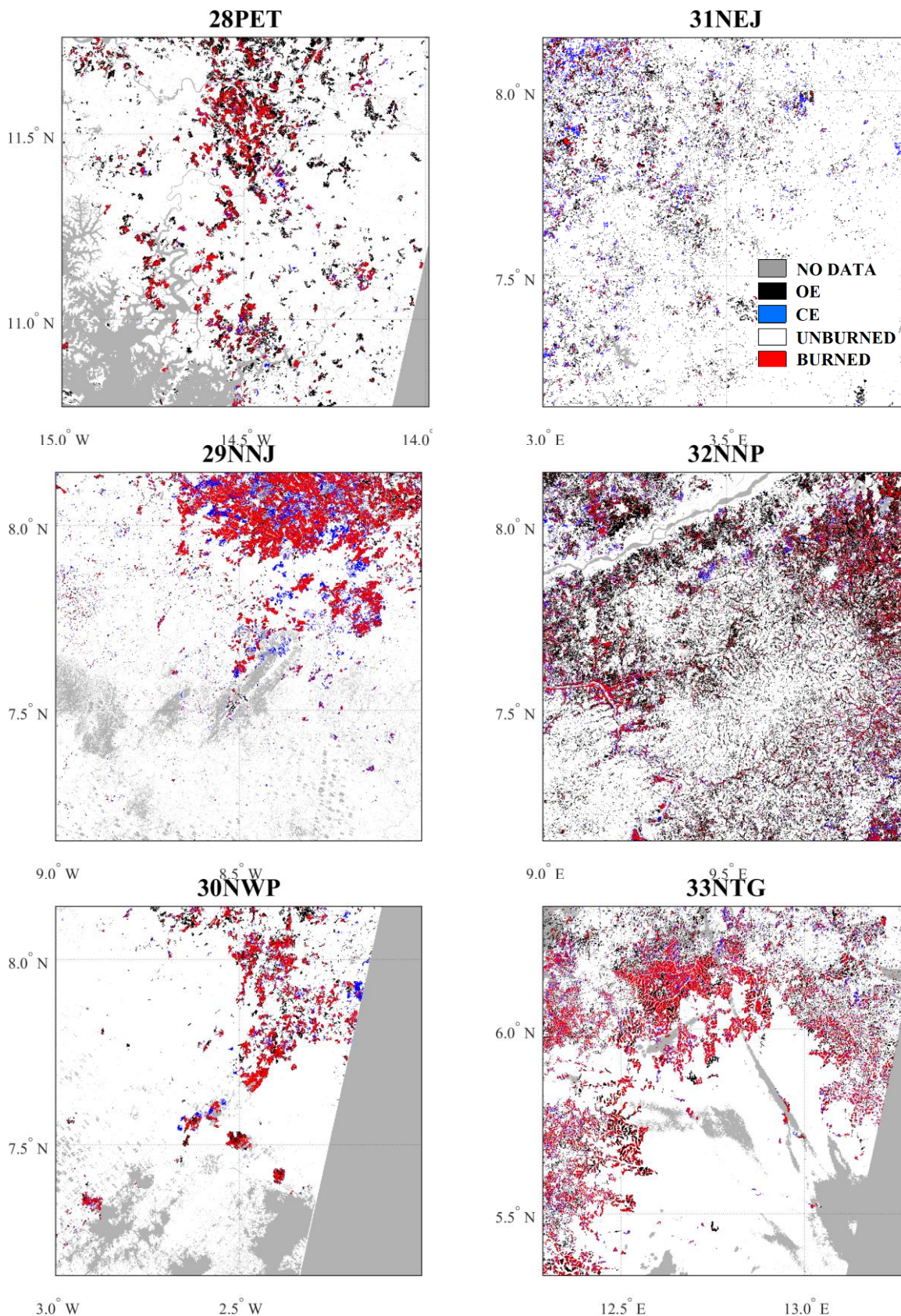
Santoro, M., Kirches, G., Wevers, J., Boettcher, M., Brockmann, C., Lamarche, C., Bontemps, S., & Defourny, P. (2017). Land Cover Product User Guide Version 2.0 (CCI-LC-PUGv2). In. Available at: https://www.esa-landcover-cci.org/?q=webfm_send/112



Annex 1: Acronyms and abbreviations

AC	Anomalous Changes
ATBD	Algorithm Theoretical Basis Document
BA	Burned Area
BAMS	Burned Area Mapping Software
CE	Commission error
DC	Dice coefficient
EHU	University of the Basque Country
GRD	Ground Range Detected
IBC	Initial Burned Confirmed
MGRS	Military Grid Reference System
MIRBI	Mid-Infrared Burned Index
MODIS	Moderate Resolution Imaging Spectroradiometer
NBR	Normalized Burned Ratio 2
NIR	Near Infrared
OE	Omission error
RD	Reference Document
relB	Relative Bias
RF	Random forest
RSS	Remote Sensing Solutions GmbH
S-1	Sentinel-1
S-2	Sentinel-2
SAR	Synthetic Aperture Radar
SFD	Small Fires Database
SWIR	Short Wave Infrared
TRMM	Tropical Rainfall Measuring Mission
UAH	University of Alcala
UL	University of Leicester
VIIRS	Visible Infrared Imaging Radiometer Suite

Annex 2a: BA detected by tiles, UAH algorithm. OE and CE errors are shown.





fire
cci

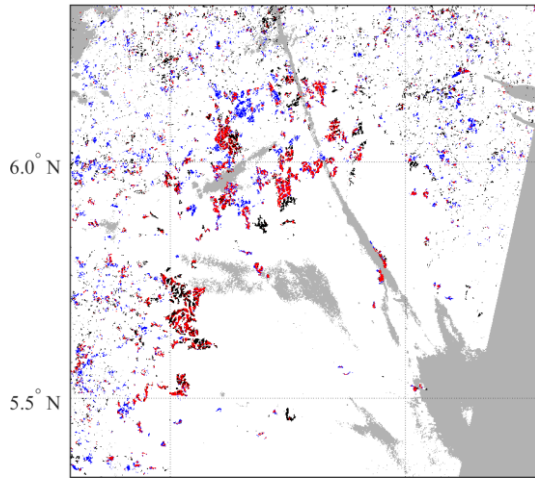
Fire_cci
Algorithm inter-comparison document

Ref.: Fire_cci_O3.D5_AID-SFD-SA_v1.1

Issue 1.1 Date 30/10/2018

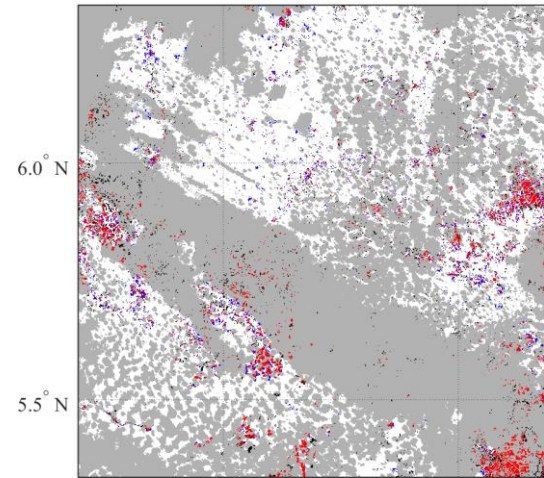
Page 20

33NTGb



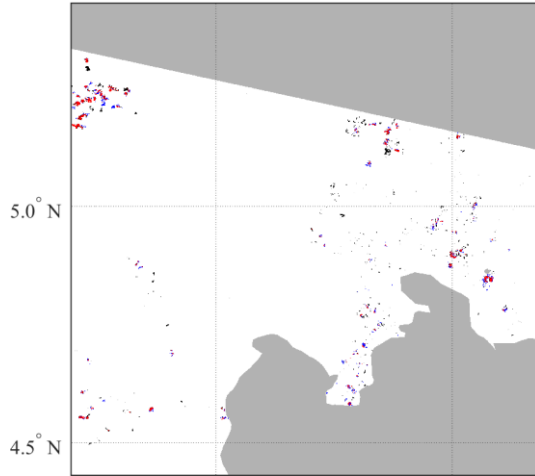
12.5° E 13.0° E

33NUGb



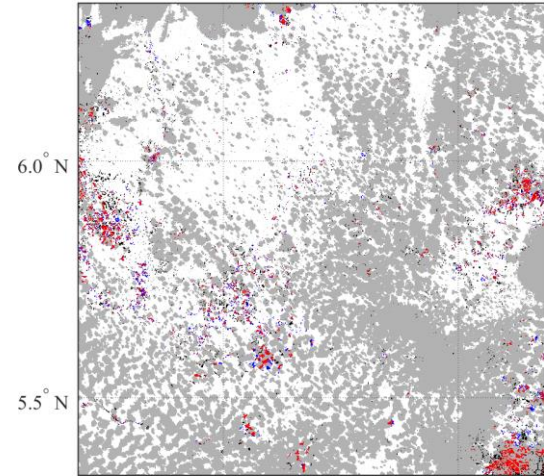
13.5° E 14.0° E

33NUF



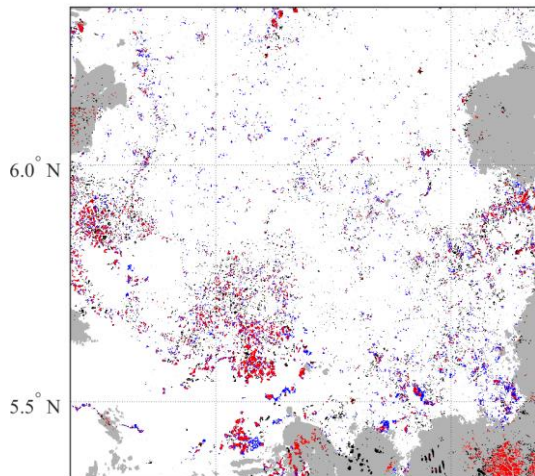
13.5° E 14.0° E

33NUGc



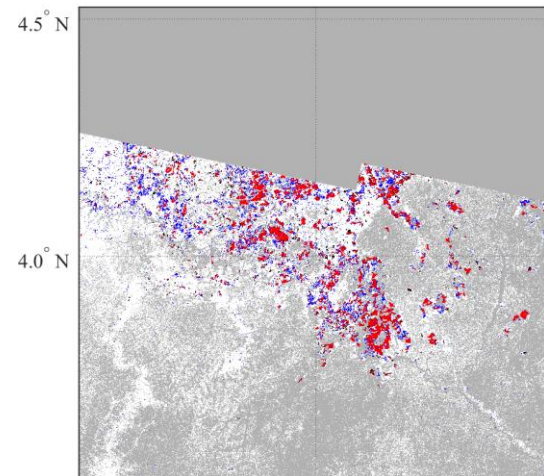
13.5° E 14.0° E

33NUG



13.5° E 14.0° E

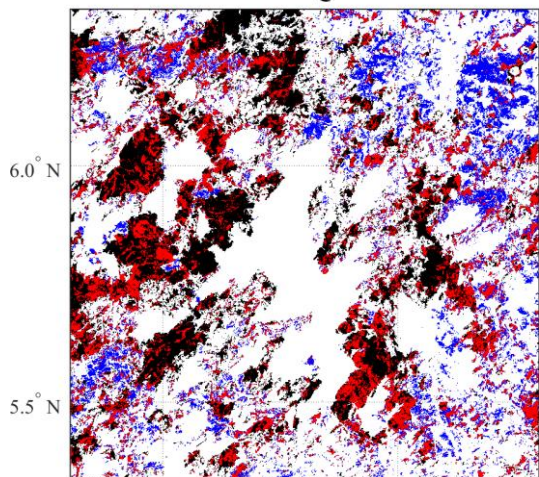
33NWE



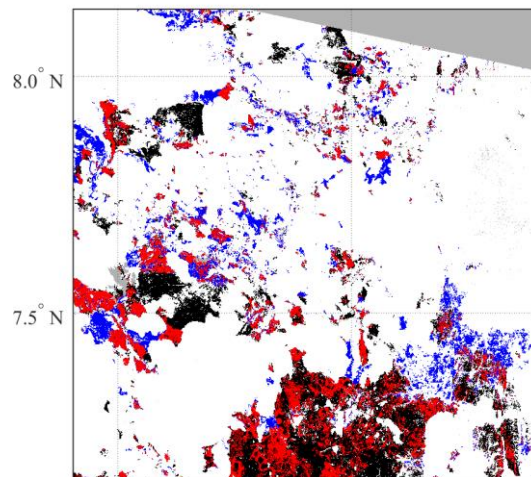
15.0° E 15.5° E



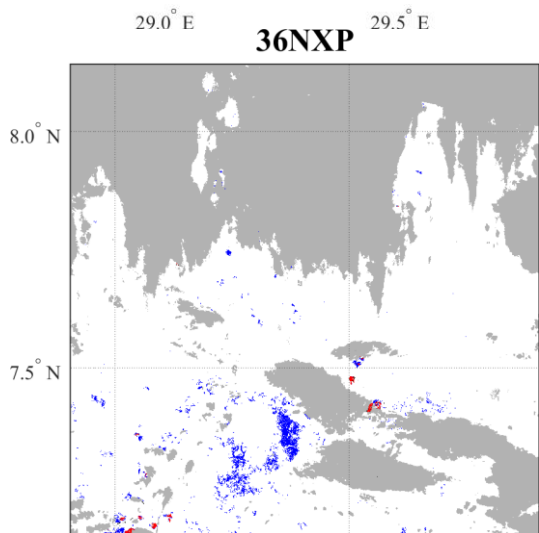
35NQG



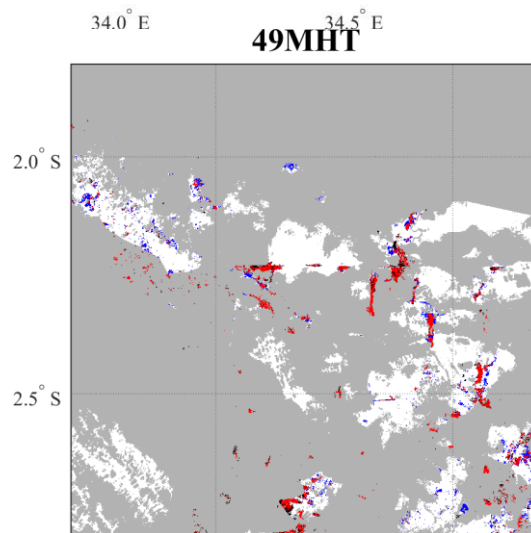
36NXPb



36NXP

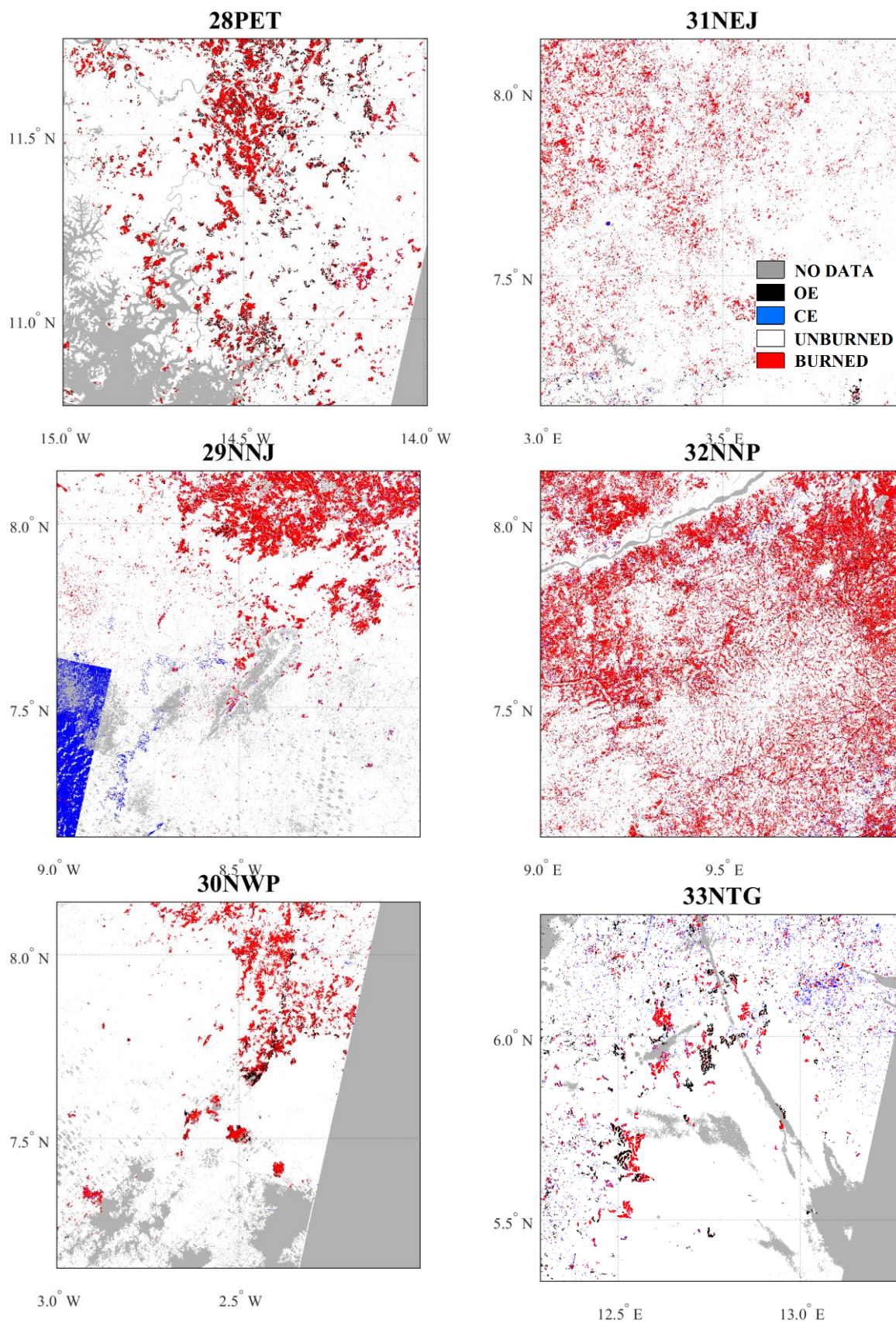


49MHT

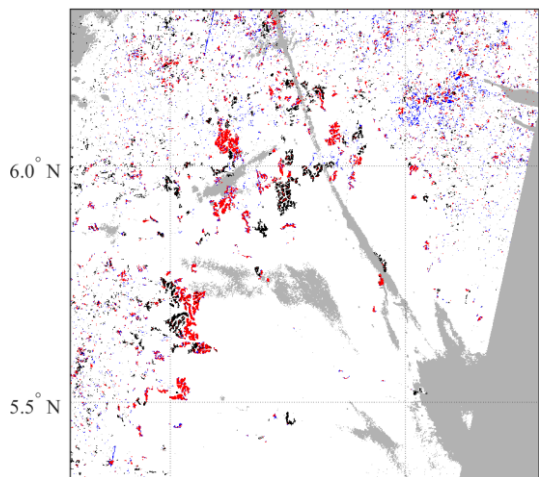


* letters in the tile name indicate different detection periods as per Table 3

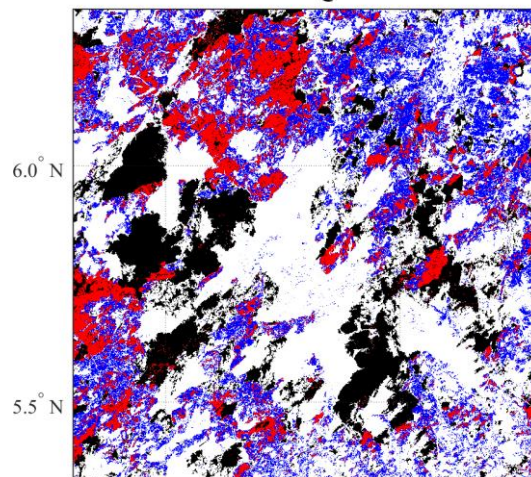
Annex 2b: BA detected by tiles, EHU algorithm. OE and CE errors are shown.



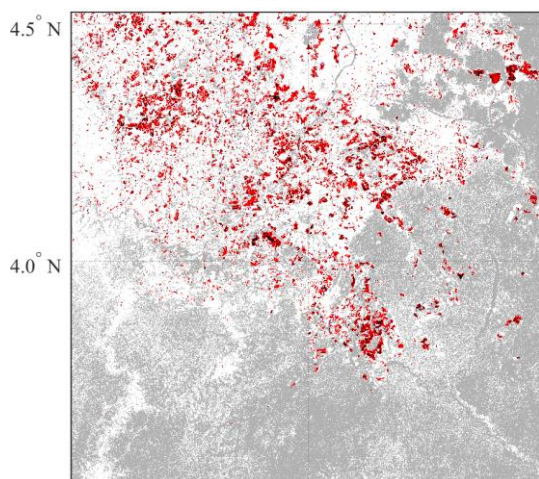
33NTGb



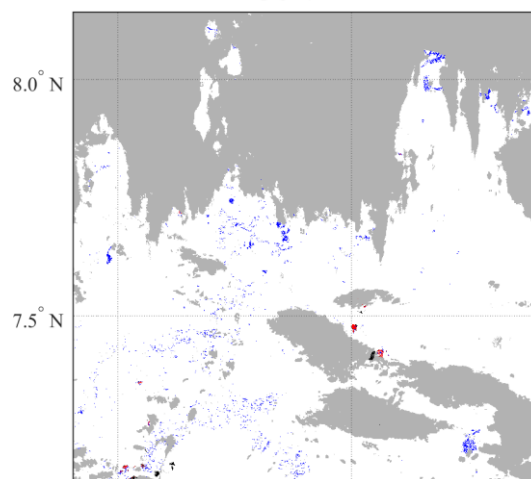
35NQG



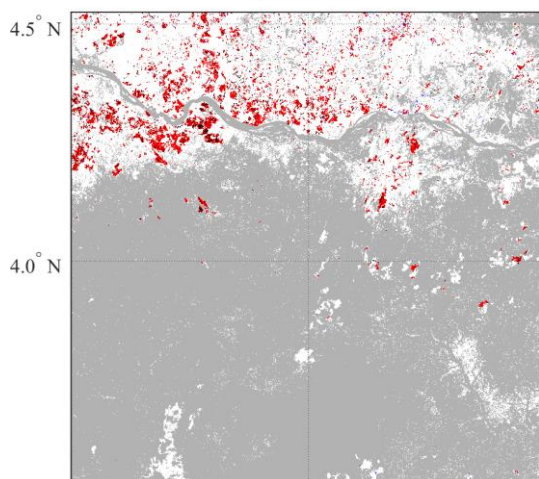
12.5° E **33NWE** 13.0° E



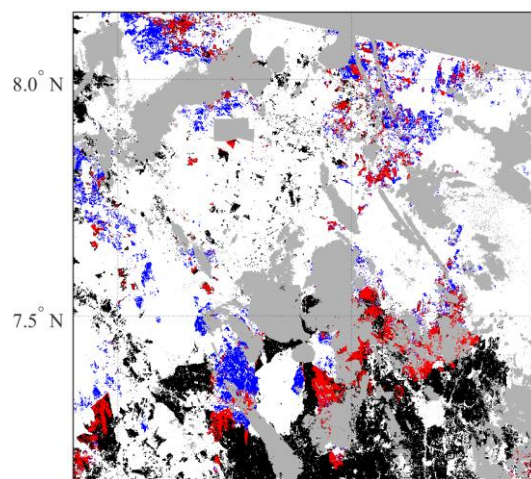
29.0° E **36NXP** 29.5° E



15.0° E **34NEK** 15.5° E



34.0° E **36NXPc** 34.5° E

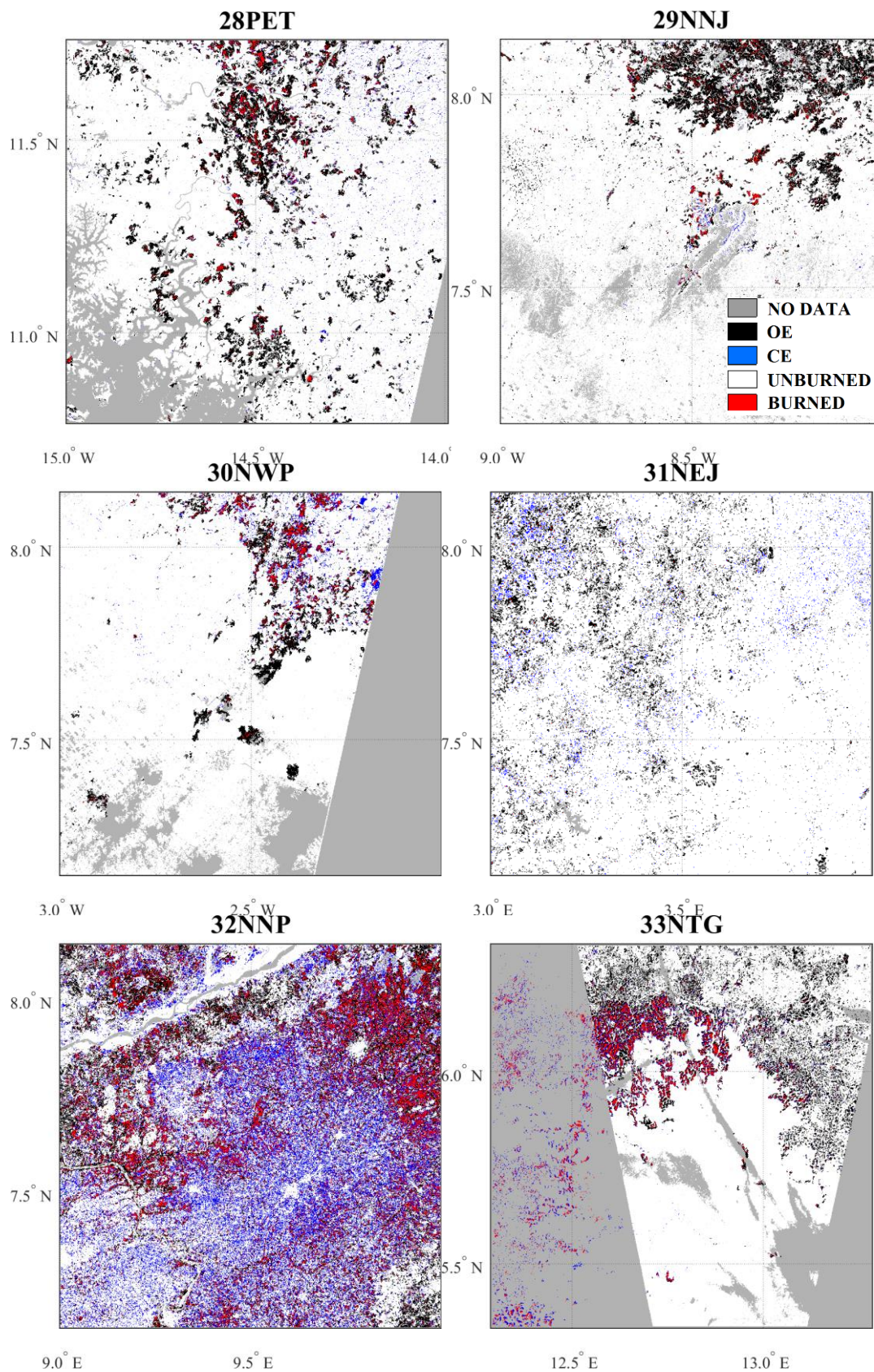


21.0° E 21.5° E

34.0° E 34.5° E

* letters in the tile name indicate different detection periods as per Table 3

Annex 2c: BA detected by tiles, UL algorithm. OE and CE errors are shown.





fire
cci

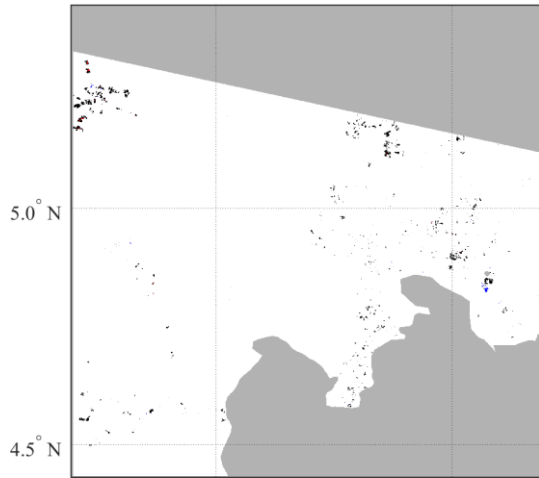
Fire_cci
Algorithm inter-comparison document

Ref.: Fire_cci_O3.D5_AID-SFD-SA_v1.1

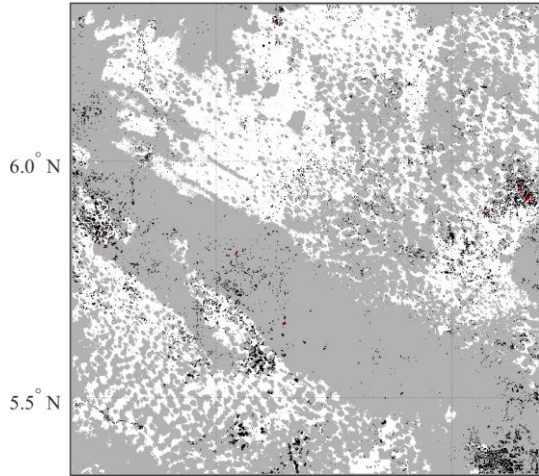
Issue 1.1 Date 30/10/2018

Page 25

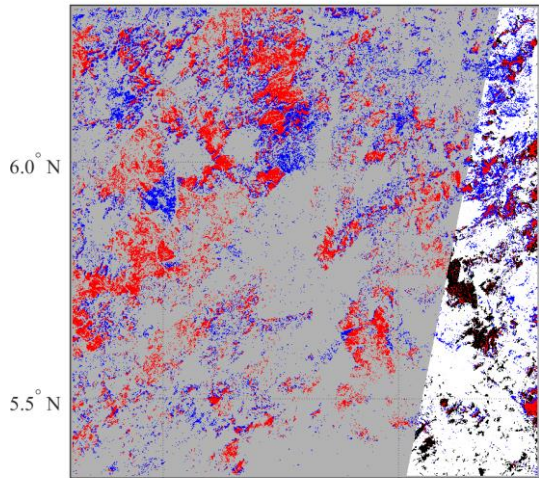
33NUF



13.5° E 14.0° E
33NUGb

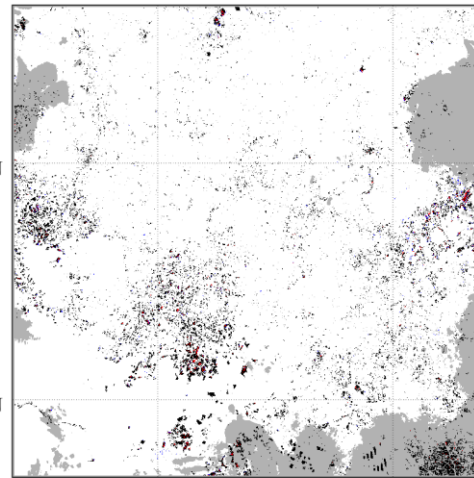


13.5° E 14.0° E
35NQG

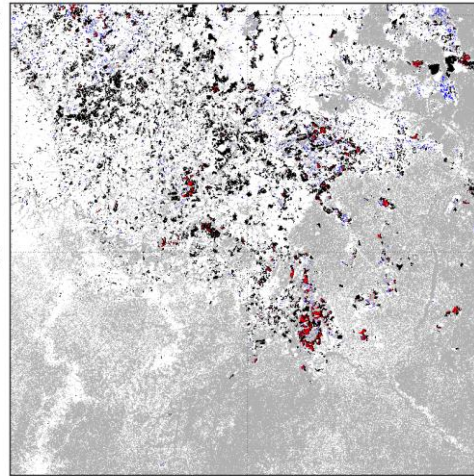


29.0° E 29.5° E

33NUG



13.5° E 14.0° E
33NWE



15.0° E 15.5° E
36NXP



34.0° E 34.5° E

Annex 2d: BA detected by tiles, RSS algorithm. OE and CE errors are shown.

